RNF168 regulates R-loop resolution and genomic stability in BRCA1/2-deficient tumors

Parasvi S. Patel,[1] Karan Joshua Abraham,[2] Kiran Kumar Naidu Guturi,[1] Marie-Jo Halaby,[1] Zahra Khan,[1] Luis Palomero,[3] Brandon Ho,[4] Shili Duan,[1] Jonathan St-Germain,[1] Arash Algouneh,[2] Francesca Mateo,[3] Samah El Ghamrasni,[1] Haithem Barbour,[5] Daniel R. Barnes,[6] Jonathan Beesley,[7] Otto Sanchez,[8] Hal K. Berman,[9] Grant W. Brown,[4] El Bachir Affar,[5] Georgia Chenevix-Trench,[7] Antonis C. Antoniou,[6] Cheryl H. Arrowsmith,[1] Brian Raught,[1] Miquel Angel Pujana,[3] Karim Mekhail,[2] Anne Hakem,[1] and Razqallah Hakem[1,2]

[1]Princess Margaret Cancer Centre, University Health Network and Department of Medical Biophysics, and [2]Department of Laboratory Medicine and Pathobiology, University of Toronto, Toronto, Ontario, Canada. [3]Program Against Cancer Therapeutic Resistance (ProCURE), Catalan Institute of Oncology (ICO), Bellvitge Institute for Biomedical Research (IDIBELL), L'Hospitalet del Llobregat, Barcelona, Catalonia, Spain. [4]Department of Biochemistry and Donnelly Centre, University of Toronto, Toronto, Ontario, Canada. [5]Centre de Recherche, Hôpital Maisonneuve-Rosemont, Montreal, Quebec, Canada. [6]Centre for Cancer Genetic Epidemiology, Department of Public Health and Primary Care, University of Cambridge, Cambridge, United Kingdom. [7]Cancer Division, QIMR Berghofer Medical Research Institute, Brisbane, Queensland, Australia. [8]University of Ontario Institute of Technology, Oshawa, Ontario, Canada. [9]Toronto General Research Institute, Toronto, Ontario, Canada.

Germline mutations in *BRCA1* and *BRCA2* (*BRCA1/2*) genes considerably increase breast and ovarian cancer risk. Given that tumors with these mutations have elevated genomic instability, they exhibit relative vulnerability to certain chemotherapies and targeted treatments based on poly (ADP-ribose) polymerase (PARP) inhibition. However, the molecular mechanisms that influence cancer risk and therapeutic benefit or resistance remain only partially understood. BRCA1 and BRCA2 have also been implicated in the suppression of R-loops, triple-stranded nucleic acid structures composed of a DNA:RNA hybrid and a displaced ssDNA strand. Here, we report that loss of RNF168, an E3 ubiquitin ligase and DNA double-strand break (DSB) responder, remarkably protected *Brca1*-mutant mice against mammary tumorigenesis. We demonstrate that RNF168 deficiency resulted in accumulation of R-loops in *BRCA1/2*-mutant breast and ovarian cancer cells, leading to DSBs, senescence, and subsequent cell death. Using interactome assays, we identified RNF168 interaction with DHX9, a helicase involved in the resolution and removal of R-loops. Mechanistically, RNF168 directly ubiquitylated DHX9 to facilitate its recruitment to R-loop–prone genomic loci. Consequently, loss of RNF168 impaired DHX9 recruitment to R-loops, thereby abrogating its ability to resolve R-loops. The data presented in this study highlight a dependence of BRCA1/2-defective tumors on factors that suppress R-loops and reveal a fundamental RNF168-mediated molecular mechanism that governs cancer development and vulnerability.

Introduction

Germline-deleterious mutations in *BRCA1* and *BRCA2* (*BRCA1/2*) predispose to high lifetime risks of breast and ovarian cancer (1). BRCA1/2 are essential for DNA double-strand break (DSB) repair through homologous recombination (2). Emerging resistance to standard chemotherapy has led to the introduction of poly (ADP-ribose) polymerase inhibition (PARPi) as a therapy for *BRCA1/2*-mutated cancers. However, resistance to PARPi through various molecular mechanisms has been documented (1), and thus identification of additional novel therapeutic targets for BRCA1/2-deficient tumors remains of utmost importance.

DNA-RNA hybrids, or R-loops, are 3-stranded nucleic acid structures comprising a DNA:RNA duplex and a displaced ssDNA

(3). These structures are generated when a nascent RNA strand infiltrates the DNA duplex behind the RNA polymerase. While R-loops are a naturally occurring consequence of transcription, persistent R-loop accumulation can compromise genomic integrity by exposing ssDNA to nicks and other types of damage, which can thereby impair transcription, cause replication stress, and lead to premature senescence (3–7). In parallel with their role in DSB repair, BRCA1/2 are crucial to maintaining genomic integrity by regulating R-loops (8–10). The mammary glands of *BRCA1* mutation carriers display accumulated R-loops in luminal progenitor cells (11), a subpopulation that has been linked to the origin of BRCA1-associated cancers (12). Depletion of BRCA1 or its interacting helicase SETX results in the accumulation of R-loops at 3′ transcription termination pause sites (8), whereas BRCA2 deficiency causes the accumulation of R-loops at promoter-proximal pause sites (10).

Therapeutic intervention at the level of DNA repair pathways has previously been proposed to increase genomic instability and counter *BRCA1/2*-mutant and homologous recombination–deficient (HRD) cancers (13). Given that R-loop accumulation contributes to genomic instability (5), exacerbating R-loop levels
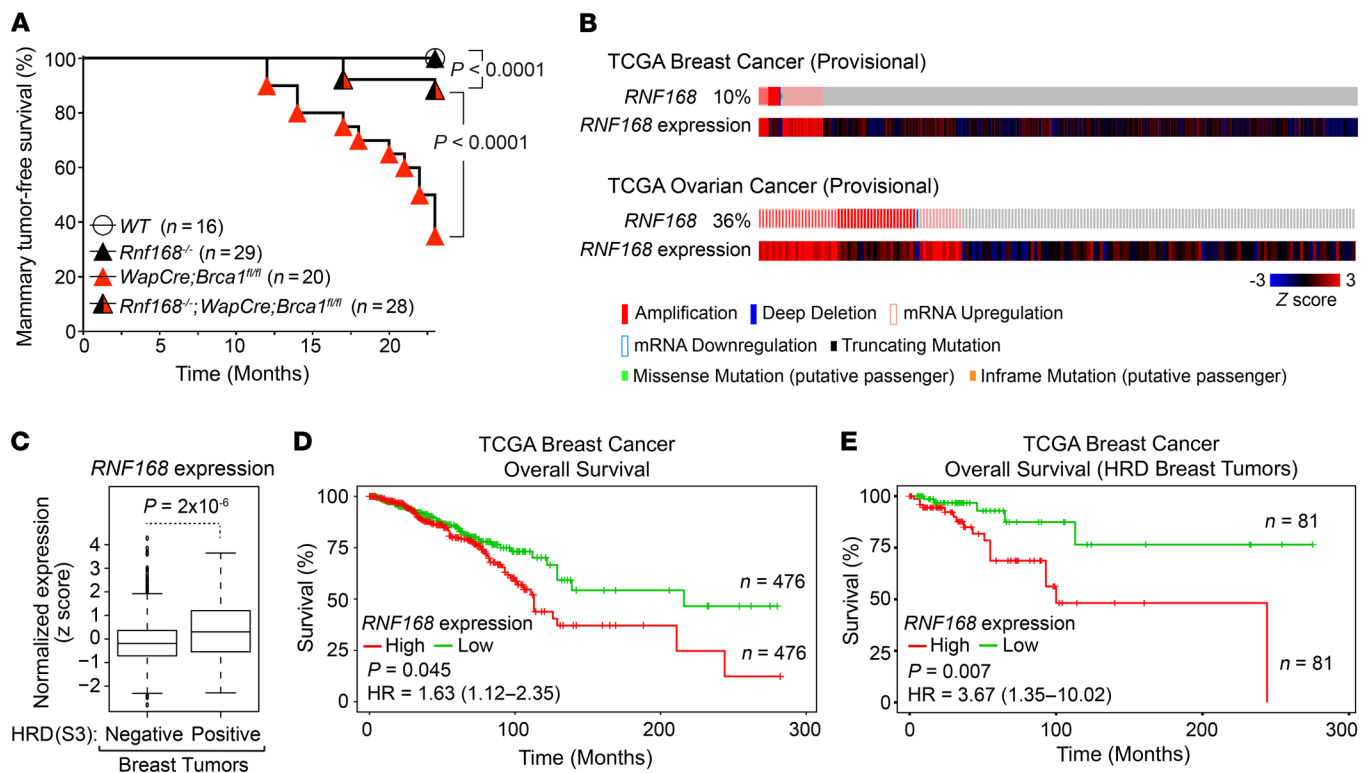
Figure 1. Loss of RNF168 protects against mammary tumorigenesis associated with *Brca1* mutations, and low expression level of human *RNF168* is associated with improved survival of patients with breast cancer who have homologous recombination deficiency. (**A**) Kaplan-Meier plot of the mammary tumor–free survival curve of cohorts of WT (*n* = 16), *Rnf168⁻/⁻* (*n* = 29), *Wap-Cre Brca1^fl/fl^* (*n* = 20), and *Rnf168⁻/⁻;Wap-Cre Brca1^fl/fl^* (*n* = 28) female mice. (**B**) Oncoprint depicting the *RNF168* status in TCGA breast and ovarian cancer datasets. (**C**) Box-and-whisker plot showing the *RNF168* expression levels in tumors negative (*n* = 874) and positive (*n* = 151) for mutational signature 3, which is linked to the HRD status. (**D**) Kaplan-Meier plot of overall survival of patients with breast cancer with high (*n* = 476) or low (*n* = 476) levels of *RNF168* expression. (**E**) Kaplan-Meier plot of relapse-free survival of patients with breast cancer with HRD tumors divided into high-level (*n* = 81) and low-level (*n* = 81) *RNF168* expression groups. The *P* values correspond to log-rank tests. The HR is indicated for **D** and **E**. For **D** and **E**, a log-rank test was performed; the top and bottom tertiles are shown. For **C**, a 2-tailed, unpaired Student's *t* test was performed.

may be an exploitable vulnerability for BRCA1/2-deficient cancers. RNF168 is an E3 ubiquitin ligase that recruits BRCA1 and the nonhomologous end joining (NHEJ) mediator TP53BP1 to DSBs. Loss of TP53BP1 has been reported to rescue homologous recombination defects and mammary tumorigenesis associated with *BRCA1* mutations (14, 15). Given that RNF168 loss impairs recruitment of TP53BP1 to DSBs and affects its function (16, 17), we examined the effect of RNF168 deficiency on cancers associated with *BRCA1/2* deficiency. In this study, we demonstrated that loss of RNF168 in BRCA1/2-deficient cells impaired the recruitment of the DNA:RNA duplex-resolving helicase DHX9 to R-loops, thereby leading to R-loop accumulation, subsequent replication stress, genomic instability, and loss of viability. Collectively, our data support targeting RNF168 alone and its potential concomitant inhibition with current treatment modalities to treat patients with BRCA1/2-deficient tumors.

Results

RNF168 depletion in BRCA1-null mouse models protects against mammary tumorigenesis. RNF168 is important for the recruitment to DSBs of TP53BP1, a factor that promotes NHEJ repair of DSBs (16, 17). In *Brca1*-mutant mouse models, deficiency of Trp53bp1 restores homol-

ogous recombination–mediated DSB repair and protects these mice from mammary tumorigenesis (14, 15). To investigate the relationship between RNF168, BRCA1, and breast cancer, we examined female mice deficient for BRCA1 in mammary epithelial cells (*Wap-Cre Brca1^fl/fl^*, ref. 18), *Rnf168⁻/⁻* mutants (19), *Rnf168⁻/⁻ Wap-Cre Brca1^fl/fl^* double KO (DKO) females, and WT littermates. *Brca1^fl/fl^* cells carry *loxP* sites flanking *Brca1* exons 5 and 6, and deletion of these exons results in a null *Brca1* mutation (20, 21). Western blot analysis using antibodies that recognize full-length BRCA1 failed to detect expression of full-length BRCA1 or truncated proteins in mammary tumor cells from *Wap-Cre Brca1^fl/fl^* mice and in *Brca1^fl/fl^* mouse embryonic fibroblasts (MEFs) after Cre-mediated deletion of exons 5 and 6 (21).

To determine the effect of RNF168 depletion on mammary tumorigenesis associated with *Brca1* mutation, cohorts of DKO female mice, their single KO (SKO; *Rnf168⁻/⁻* and *Wap-Cre Brca1^fl/fl^*) counterparts, and WT littermates were monitored for 23 months for mammary tumor development. As previously reported (18), approximately 65% of *Wap-Cre Brca1^fl/fl^* females developed mammary tumors between 12 and 23 months of age (Figure 1A). Strikingly, only 11% of DKO females developed mammary tumors (Figure 1A). These findings revealed that *Rnf168* deletion in *Brca1*-null mouse models protected against mammary tumorigenesis.
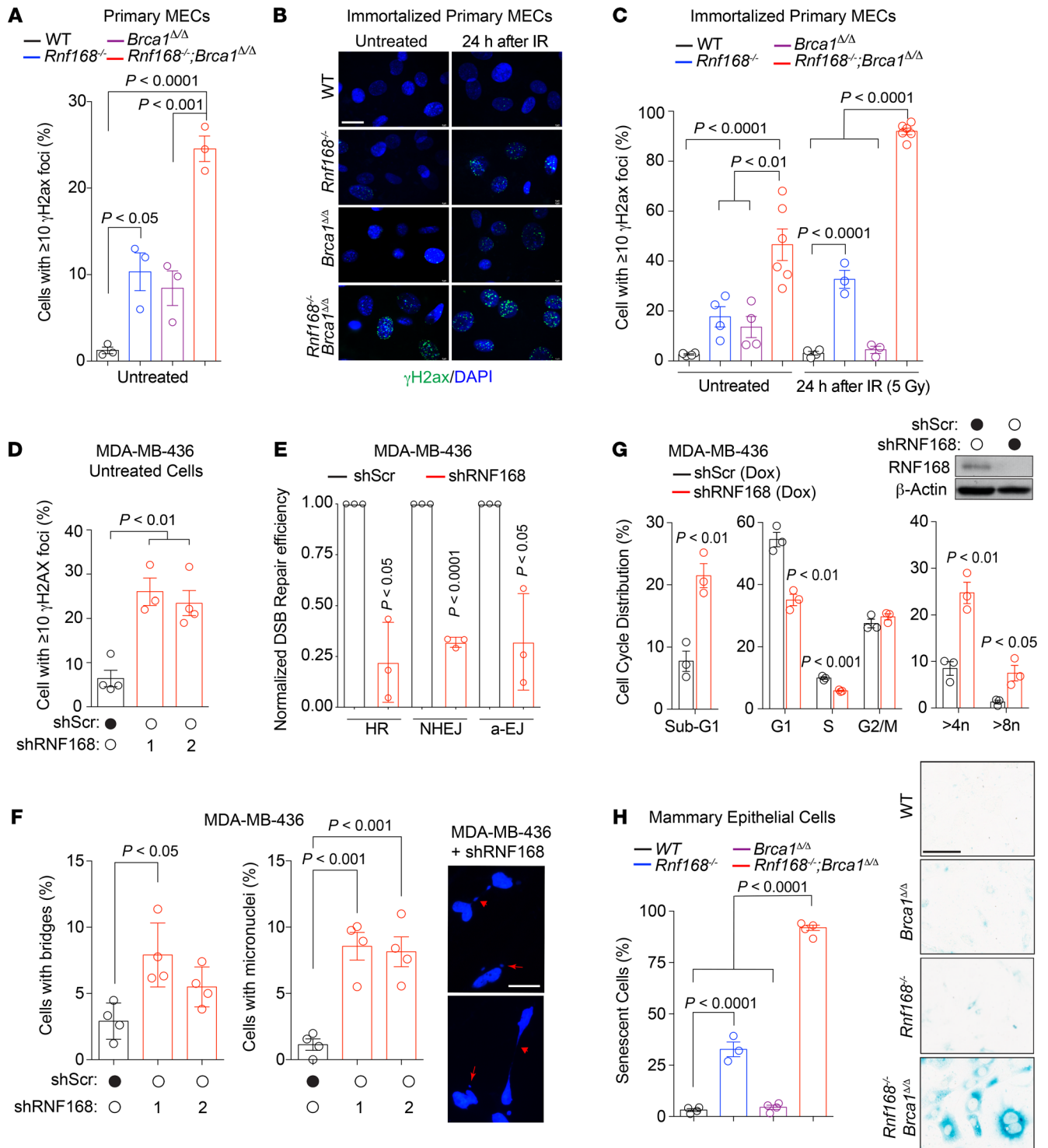
Figure 2. Loss of RNF168 increases genomic instability, impairs DSB repair, and causes senescence in BRCA1-deficient cells. (**A**) Quantification of primary MECs with the indicated genotypes exhibiting 10 or more spontaneous γH2AX foci ($n = 3$). (**B**) Representative images of γH2AX staining in indicated cells under untreated or irradiated conditions. Scale bar: 50 μm. (**C**) Quantification of cells with 10 or more γH2AX foci from **B** ($n = 3–6$). (**D**) Quantification of indicated cells exhibiting 10 or more spontaneous γH2AX foci. Western blot for sh*RNF168* knockdown efficiency is shown in Supplemental Figure 5A ($n = 3–4$). (**E**) Efficiency of DSB repair pathways (homologous recombination, NHEJ, and a-EJ) in mediating the repair of I-SceI–induced DSBs in indicated cells ($n = 3$). sh*RNF168* knockdown efficiency and cell counts are shown in Supplemental Figure 5, I and J. (**F**) Quantification of chromosomal bridges and micronuclei in the indicated cells. Representative images of RNF168-depleted MDA-MB-436 cells showing chromosomal bridges (arrowhead) and micronuclei (arrow) are shown ($n = 4$). Scale bar: 25 μm. (**G**) Cell cycle distribution analysis using propidium iodide staining of the indicated cells ($n = 3$). (**H**) Representative images of SA-β-gal staining of the indicated MECs and quantification ($n = 3–6$). Scale bar: 25 μm. For all experiments, a minimum of 3 independent experiments and 100 cells per condition and genotype were scored from at least 5 fields of view. A 1-way ANOVA followed by Tukey's multiple-comparison test (**A**, **C**, and **H**), Welch's t test (**E**), unpaired Student's t test (**G**), or 1-way ANOVA followed by Dunnett's multiple-comparison (**D** and **F**) test were performed. Data are presented as the mean ± SEM.
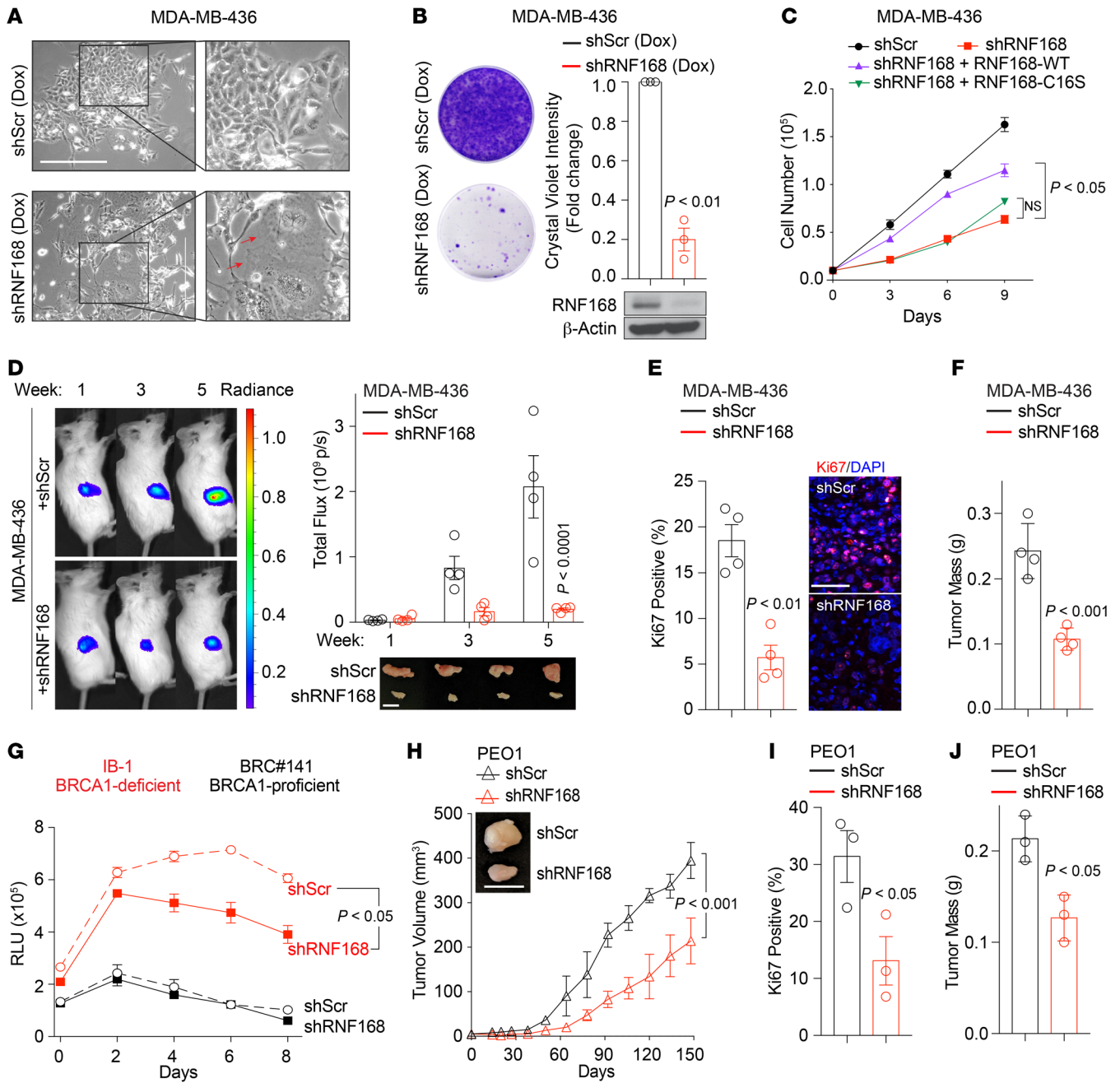
Figure 3. RNF168 depletion suppresses the in vitro and in vivo growth of BRCA1- and BRCA2-deficient breast and ovarian tumor cells, respectively. (**A**) Representative images of the indicated BRCA1-deficient cells. Scale bar: 500 μm. The arrows indicate large, flat senescent cells. (**B**) Long-term proliferation of indicated MDA-MB-436 cells stained with crystal violet; 100,000 cells were seeded per 6 cm plate; cells were fixed after 21 days ($n = 3$). (**C**) Cumulative growth curve in indicated cells ($n = 3$). (**D**) In vivo growth of indicated xenografts ($n = 4$). p/s, photons/second. Representative images are shown (scale bar: 1 cm). (**E**) Representative images of staining in tumors from **D** ($n = 4$) and quantification. Scale bar: 100 μm. (**F**) Quantification of tumor mass from the experiments in **D** and **E**. (**G**) Relative growth of the indicated TNBC PDXs ($n = 3$). RLU, relative luciferase unit. (**H**) In vivo growth of *BRCA2*-mutant PEO1 control and RNF168-depleted xenografts. Representative images are shown ($n = 3$). Scale bar: 1 cm. (**I**) Quantification of Ki67 immunofluorescence in indicated cells. (**J**) Quantification of tumor mass from **H**. Data were analyzed by Welch's *t* test (**B**), 2-way ANOVA with Tukey's multiple-comparison test (**C**), 2-way ANOVA with Sidak's multiple-comparison test (**D**), 2-tailed, unpaired Student's *t* test (**E**, **F**, **I**, and **J**), 2-tailed, paired Student's *t* test (**G**), and 2-tailed Wilcoxon matched-pairs signed-rank test (**G**). Data are presented as the mean ± SEM.

Decreased expression of human RNF168 is associated with improved survival of patients with HRD breast cancer. Next, we explored the correlations of *RNF168* status in human cancer using data from cBioPortal (22). Levels of *RNF168* expression were found to be significantly higher in tumors from 4 cancer types, including breast cancer, than in the corresponding normal tissue (Figure 1B and Supplemental Figure 1; supplemental material, including the full, uncut gels, is available online with this article; https://
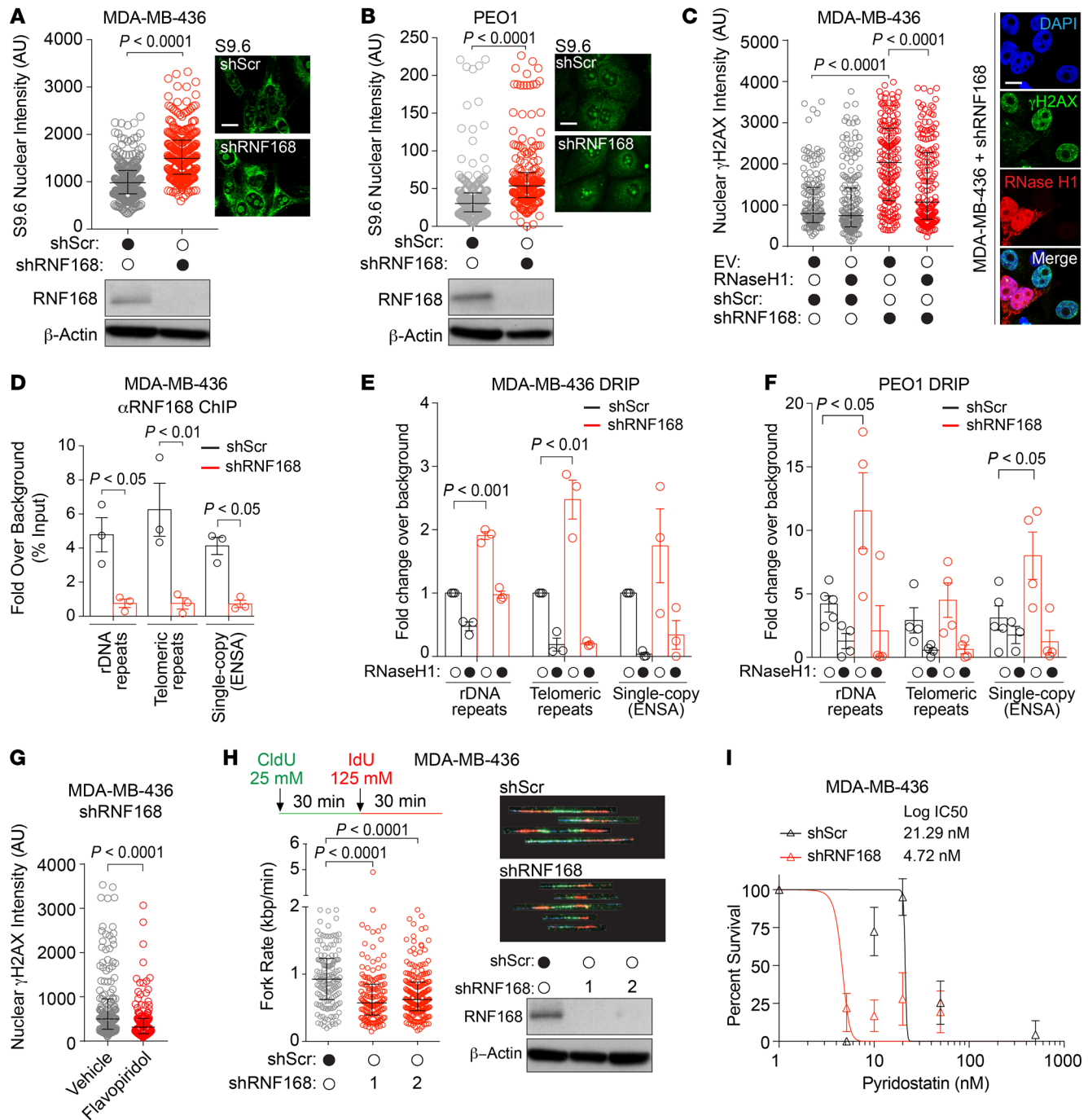
Figure 4. RNF168 suppresses the formation of R-loops in *BRCA1/2*-mutant tumors and maintains replication fork stability. (**A** and **B**) Representative images of S9.6 immunofluorescence and quantification in indicated MDA-MD-436 (**A**) and PEO1 (**B**) cells (*n* = 3). Scale bar: 10 μm. A minimum of 270 cells were scored for each cell line. (**C**) Immunofluorescence and quantification of nuclear γH2AX signals in indicated cells. Representative images are shown (*n* = 3). Scale bar: 10 μm. A minimum of 200 cells were scored for each cell line. (**D**) ChIP-qPCR analysis of RNF168 recruitment to the R-loop–prone loci in indicated cells (*n* = 3). (**E** and **F**) DRIP with or without in vitro pretreatment with RNASEH1 in indicated MDA-MB-436 (**E**) and PEO1 (**F**) cells (*n* = 3–4). (**G**) Immunofluorescence and quantification of nuclear γH2AX foci in indicated cells after short-term (2 hours) treatment with flavopiridol or vehicle control (*n* = 3). (**H**) DNA fiber assay in indicated cells. A minimum of 150 fibers were measured for each cell line (*n* = 2). (**I**) Fourteen-day dose-response survival curve in indicated cells after a single treatment with pyridostatin (*n* = 3). Data were analyzed using Mann-Whitney *U* test (**A**, **B**, and **G**), Kruskal-Wallis test with Dunn's multiple-comparison test (**C**), 2-tailed, unpaired Student's *t* test (**D**–**F**), Kruskal-Wallis test (**H**), and nonlinear regression (**I**). The vertical scatter plots show the medians and quartiles. Data are presented as the mean ± SEM.

doi.org/10.1172/JCI140105DS1). Overexpression was associated with genomic amplification in breast and ovarian cancers (Supplemental Figure 2, A–D), whereas deletion, downregulation, and/or somatic mutation were infrequent (Supplemental Figure 2, E and

F). *RNF168* was predominantly overexpressed in a basal-like subtype that included breast cancer associated with *BRCA1* mutations (Supplemental Figure 3, A and B). Higher *RNF168* expression was also observed in HRD breast tumors, classified by positivity for
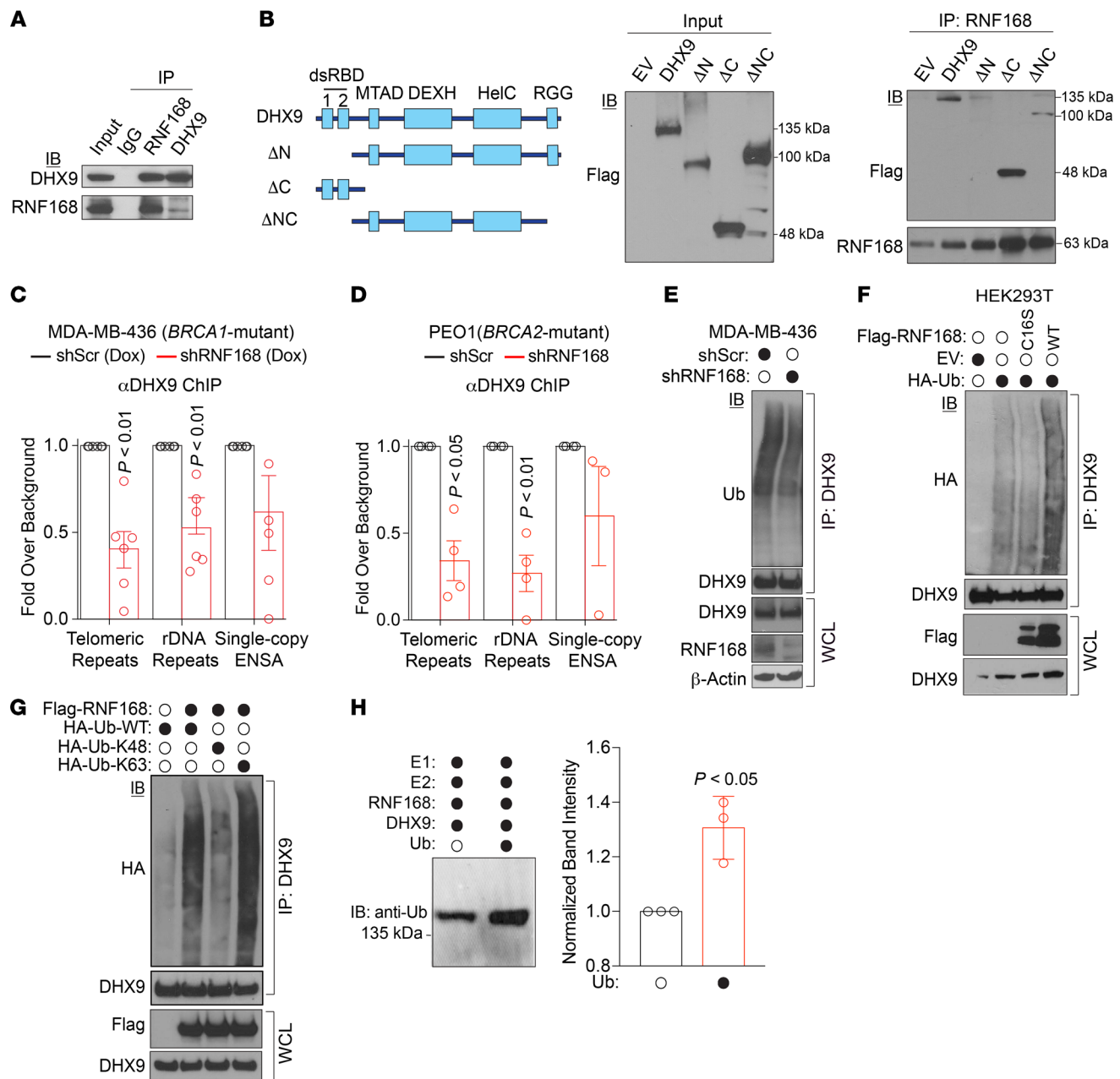
Figure 5. RNF168 ubiquitylates DHX9 in vivo and in vitro and controls its recruitment to R-loop–prone loci. (**A**) Pulldown analysis of the interaction between RNF168 and the helicase DHX9 in MDA-MB-436 nuclear lysates. (**B**) Schematic of DHX9 mutants cloned into MSCV-Flag and map of DHX9 domains interacting with RNF168. (**C** and **D**) DHX9 ChIP-qPCR at R-loop–prone loci in indicated MDA-MB-436 (**C**) and PEO1 (**D**) cells (n = 3–6). (**E**) In vivo ubiquitylation of DHX9 in the indicated cells. Whole-cell lysates (WCL) were subjected to IB as indicated. (**F**) HEK293T cells were transfected with indicated Flag-tagged mouse *Rnf168*, empty vector (EV), and HA-Ub as indicated. WCL were subjected to IP with anti-DHX9 antibody and membrane was probed with anti-ubiquitin antibody. In vivo ubiquitylation of DHX9 in indicated cells is shown. (**G**) HEK293T cells were transfected with *Flag-Rnf168* and HA-Ub (WT, K48, or K63), and WCL were subjected to IP and IB as in **F**. (**H**) Western blot showing the results of the in vitro ubiquitylation reaction in the presence and absence of ubiquitin (n = 3) and quantification of Ub band intensity in the reaction containing Ub, normalized for each replicate to Ub band intensity in the reaction performed in the absence of Ub. Data were analyzed using a 2-tailed, unpaired Student's t test (**C**, **D**, and **H**). dsRBD, double-stranded RNA-binding domain; MTAD, minimal transactivation domain; DEXH, DEXH box motif; HelC, helicase domain; RGG, RGG box; ΔN, N-terminal deleted; ΔC, C-terminal deleted; and ΔNC, N- and C-terminals deleted.

the somatic mutational signature 3 (ref. 23, Figure 1C, and Supplemental Figure 3C). Kaplan-Meier survival analyses revealed that high *RNF168* expression levels were associated with poorer overall survival in patients with breast cancer (Figure 1D) and in patients with HRD breast tumors (Figure 1E).

Building on the aforementioned evidence, we analyzed genetic variants in the *RNF168* locus for modification of breast cancer risk in human female carriers of *BRCA1/2* mutations. Using the genome-wide association study (GWAS) results generated by the OncoArray and Collaborative Oncological Gene-environment
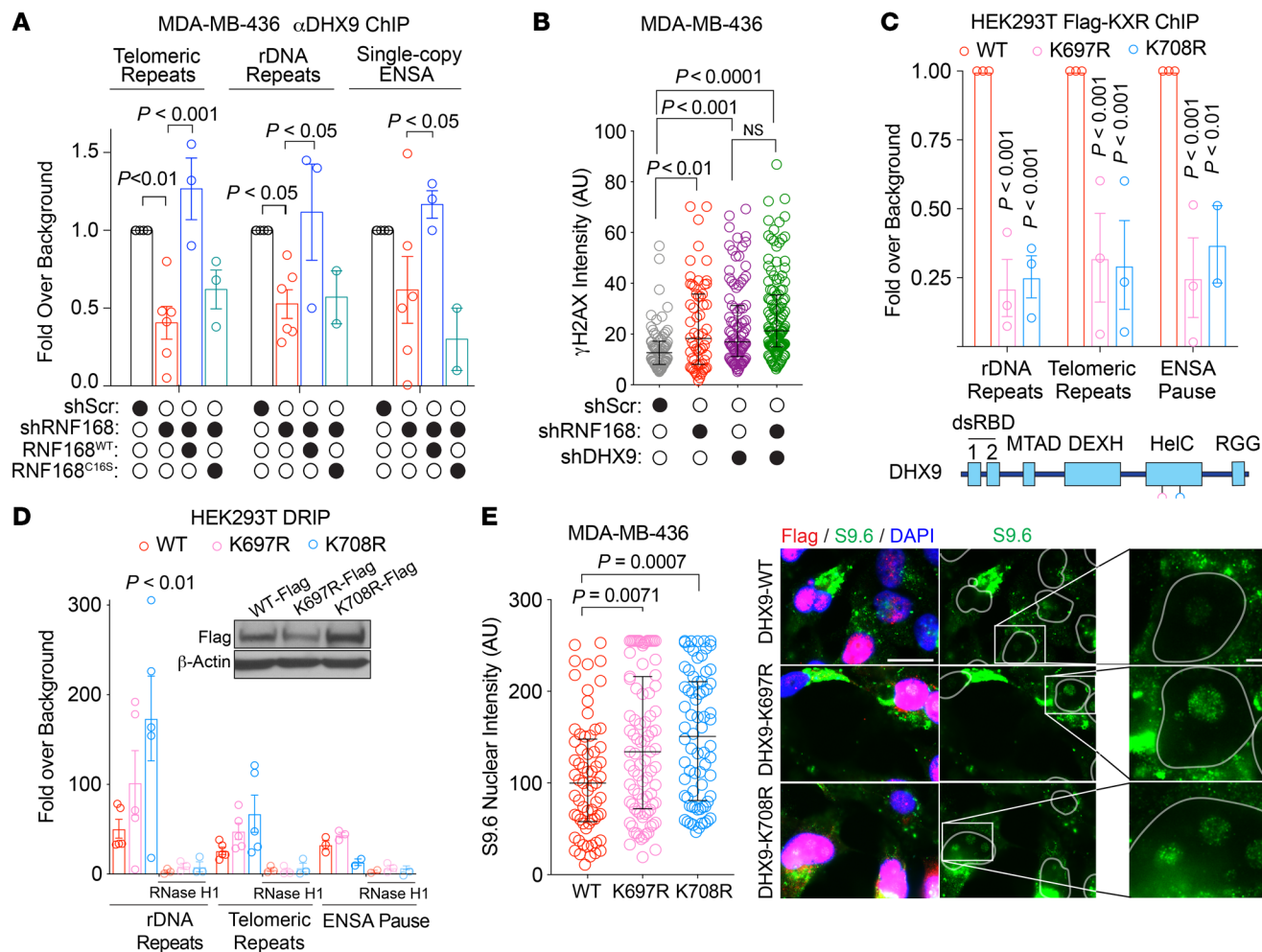
Figure 6. Complementation of RNF168-depleted cells with WT RNF168 rescues DHX9 recruitment to R-loops through the ubiquitylation of this helicase at different lysines. (**A**) Anti-DHX9 ChIP-qPCR was performed using MDA-MB-436 cells to examine the effect of RNF168-WT and its C16S mutant on the recruitment of DHX9 to R-loop–prone loci, as indicated ($n = 3$–6). (**B**) Quantification of γH2AX signal intensity in the indicated cell lines. (**C**) ChIP-qPCR using anti-Flag in HEK293T cells transfected with indicated Flag-tagged lysine to arginine (KXR) point mutants ($n = 2$–3). (**D**) DRIP-qPCR in HEK293T cells transfected with indicated Flag-tagged KXR point mutants ($n = 3$–4). Western blot for DHX9 WT and KXR expression is shown. (**E**) S9.6 immunofluorescence in MDA-MB-436 cells transfected with indicated Flag-tagged KXR point mutants. S9.6 intensity was quantified in cells transfected with Flag-tagged KXR or WT ($n = 3$). Merge bar: 20 μM; S9.6 scale bar: 5 μM. Nuclei are outlined in white. Data were analyzed using 2-way ANOVA with Tukey's multiple-comparison test (**A**), Kruskal-Wallis test with Dunn's multiple-comparison test (**B** and **E**), and 2-way ANOVA with Dunnett's multiple-comparison test (**C** and **D**). Data are presented as the mean ± SEM. For **B** and **F**, a minimum of 70 cells were quantified; the median and IQR are shown.

Study (iCOGS) and Consortium of Investigators of Modifiers of BRCA1/2 (CIMBA) projects (24–26), genotyped and imputed variants within the 150 kb segment centered on *RNF168* were examined. We identified a rare variant, rs192573104 (imputation $r^2 = 0.79$, minor allele frequency < 1% in Europeans), that associated with significantly lower breast cancer risk in *BRCA1* mutation carriers: HR = 0.68, $P = 4.3 \times 10^{-4}$ (Supplemental Table 1 and Supplemental Figure 4A). Examination of data from the Genotype-Tissue Expression (GTEx) project (27) identified rs192573104 as an expression quantitative trait locus (eQTL) for *RNF168*, with the minor allele associated with lower expression levels in several tissues (Supplemental Figure 4B). rs192573104 association with decreased cancer risk was corroborated in human carriers of *BRCA1* mutations, expected to result in a reduced transcript or protein level due to nonsense-mediated RNA decay ($n = 12,852$, HR = 0.65, 95% CI 0.50–0.85, $P = 1.3 \times 10^{-3}$).

Collectively, the obtained data indicate that deficiency of mouse or human RNF168 protects from *BRCA1* mutation–associated breast cancer and that relatively high *RNF168* expression may accelerate the progression of HRD breast cancer.

Loss of RNF168 in BRCA1-deficient cells impairs DSB repair, leading to genomic instability and senescence. Given the roles of RNF168 and BRCA1 in DSB repair (17), we examined the level of DNA damage in primary and immortalized mammary epithelial cells (MECs) from the above-described mouse models using γH2AX foci as a marker for DSBs (17). DKO MECs exhibited high levels of endogenous DSBs and severely impaired repair of irradiation-induced DSBs relative to WT and SKO controls (Figure 2, A–C). Similar observations were made in the *BRCA1*-deficient human breast cancer cell lines MDA-MB-436, HCC1937, and MDA-MB-231 transduced with shRNA targeting *RNF168* (shRNF168) and compared with control cells transduced with scrambled shRNA (shScr)
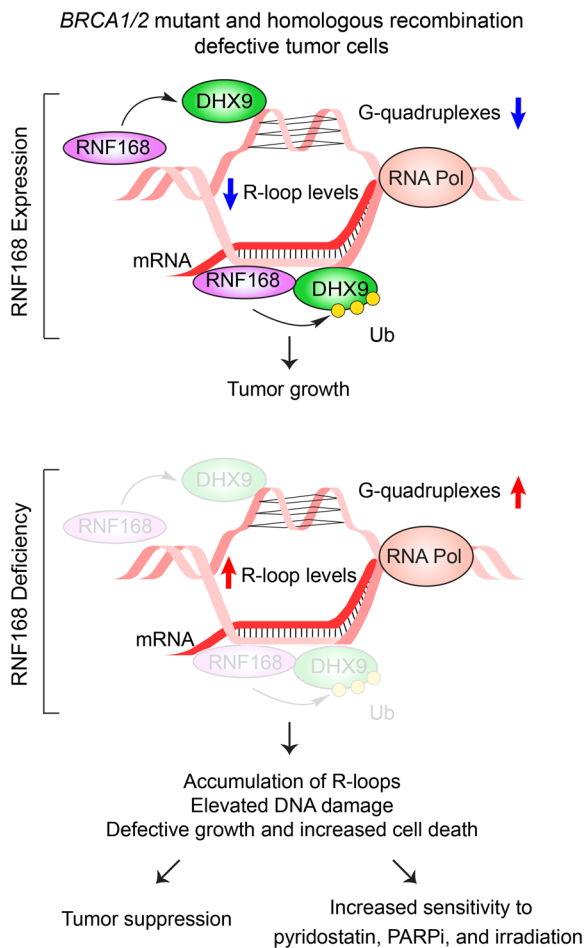
Figure 7. Schematic representation of how RNF168 and DHX9 regulate R-loop levels to control *BRCA1/2*-mutant and HRD cancers. A proposed model for the role for RNF168 in mediating DHX9 ubiquitylation and facilitating its recruitment to R-loops, leading to the resolution of these structures and decreased levels. Loss of these RNF168 functions in *BRCA1/2*-mutant and homologous recombination–deficient cells and tumors increases R-loop accumulation and DNA damage levels, leading to cell death and tumor suppression. Loss of RNF168 also increases the sensitivity of *BRCA1/2*-mutant tumors to G-quadruplexes/R-loop–stabilizing drug pyridostatin, PARP inhibitors (PARPi), and irradiation.

ity for SA-β-gal activity and senescence marker $p21^{CIP1}$ expression compared with corresponding control cells (Supplemental Figure 6C). Similar observations were made in MEFs with concurrent depletion of RNF168 and BRCA1 (Supplemental Figure 6D). Collectively, these data indicate an important role for RNF168 in facilitating DSB repair and restraining genomic instability and senescence levels in *BRCA1*-mutant cells.

Loss of RNF168 suppresses in vitro and in vivo growth of BRCA1/2-deficient tumors and increases their sensitivity to PARP inhibitors. Following up on increased genomic instability and senescence observed in the absence of BRCA1 and RNF168, we sought to examine the effect of dual loss of these proteins on in vitro and in vivo proliferation. MDA-MB-436 cells and *Brca1$^{-/-}$* mouse mammary tumor cells depleted of RNF168 had impaired long-term colony formation ability (Figure 3B and Supplemental Figure 6E). Next, because RNF168 is an E3 ligase required for DSB signaling (17), the impact of loss of its ubiquitylation activity on *BRCA1* mutant cells was also evaluated. Indeed, the growth defect in RNF168-depleted MDA-MB-436 cells was partially rescued after reconstitution with RNF168-WT, but not with the E3 ligase–dead C16S mutant (Figure 3C and Supplemental Figure 6F).

To assess the effect of RNF168 depletion on the in vivo growth of *BRCA1*-mutant breast cancer cells, MDA-MB-436 parental cells and their RNF168-depleted counterparts were xenotransplanted into the mammary fat pads of nonobese diabetic/severe combined immunodeficiency gamma (NSG) mice. Tumor growth (Figure 3D), the frequency of Ki67-positive proliferating cancer cells (Figure 3E), and tumor mass (Figure 3F) were significantly reduced with deficiency for RNF168. In further preclinical experiments, ex vivo assays using cancer cells from 2 different triple-negative breast cancer (TNBC) patient-derived xenografts (PDXs), BRC 141 (*BRCA1* WT) and IB-1 (*BRCA1* mutant; c.302-1G > A), showed that RNF168 depletion impaired the growth of *BRCA1*-mutant breast cancer cells (Figure 3G and Supplemental Figure 6G). It should be noted that if a hypomorph RING-less BRCA1 protein is being expressed in IB-1 cells, the observed growth difference may be due to the restoration of homologous recombination in these cells.

Similar to BRCA1, BRCA2 is required for homologous recombination–mediated DSB repair and is functionally relevant in breast and ovarian cancers (32). However, BRCA1 and BRCA2 functions in DSB repair are noninterchangeable, and they also have functions that are outside of their role in the canonical homologous recombination–mediated pathway of DSB repair (2, 33). Therefore, we next examined the impact of RNF168 loss on *BRCA2*-mutant ovarian cancer PEO1 cells. Compared with the parental cells, RNF168-depleted PEO1 cells exhibited increased levels of

(Figure 2D and Supplemental Figure 5, A–F). Consistent with previous reports (16, 17), depletion of RNF168 in MDA-MB-436 cells resulted in severely impaired formation of TP53BP1 foci (Supplemental Figure 5, G and H). DSB repair pathways in the context of dual loss of BRCA1 and RNF168 were further characterized using reporter assays (28, 29). We found that RNF168 depletion in MDA-MB-436 cells significantly decreased the efficiency of the homologous recombination, NHEJ, and alternative end joining (a-EJ) DSB repair (Figure 2E and Supplemental Figure 5, I and J). Furthermore, MDA-MB-436 cells depleted of RNF168, as well as DKO MECs and MEFs, exhibited an increased frequency of genomic aberrations, including chromosomal bridges and micronuclei (Figure 2F and Supplemental Figure 6, A and B). These results highlight the requirement of RNF168 for the suppression of DSBs and genomic instability associated with BRCA1 deficiency.

We further explored the effects of combined RNF168/BRCA1 deficiency on cellular homeostasis (30). DNA content analysis of RNF168-depleted MDA-MB-436 cells revealed an increase in the sub-G1 population, indicative of cell death, and elevated frequency of polyploidy (Figure 2G). Compared to controls, MECs lacking RNF168 and BRCA1 were more senescent, as quantified by β-galactosidase (SA-β-gal) activity (Figure 2H). Consistently, RNF168-depleted MDA-MB-436 cells displayed flat and vacuolated cell morphology (Figure 3A), reflecting increased senescence (31). In addition, these cells displayed significantly higher positiv-

spontaneous DSBs (Supplemental Figure 7, A and B), decreased colony-forming capacity (Supplemental Figure 7C), impaired growth as tumor xenografts (Figure 3H), decreased proliferation (Ki67+; Figure 3I), and decreased tumor mass (Figure 3J). Notably, depletion of RNF168 in *BRCA2*-mutant PEO1 ovarian cancer cells and *BRCA1*-mutant MDA-MB-436 breast cancer cells resulted in enhanced sensitivity to the PARP inhibitor olaparib (Supplemental Figure 7, D and E). Thus, in addition to suppressing tumorigenesis associated with *BRCA1/2* mutations, loss of RNF168 function also enhanced sensitivity to DNA damage–targeting therapies in *BRCA1/2*-mutant cancer cells. Collectively, these findings indicate that RNF168 function is required for in vitro and in vivo proliferation of *BRCA1* and *BRCA2* mutant breast and ovarian cancer cells, respectively.

RNF168 suppresses R-loops and replication stress associated with BRCA1/2 mutations. The above results identified RNF168 as a critical factor in *BRCA1/2*-associated tumorigenesis. To decipher the mechanism underlying this potentially novel RNF168 function, its protein interactions were examined by an immunoaffinity purification/mass spectrometry approach from Flag-RNF168– and Flag control–expressing HEK293T cells. Examination of mass spectrometry results identified DNA-RNA helicase DHX9 as a putative RNF168 interactor (Supplemental Table 2).

Intriguingly, DHX9 has an experimentally verified role in maintaining genome stability via enzymatic removal of R-loops and G-quadruplex (G4) structures (34, 35). Loss of BRCA1 or BRCA2 promotes the formation of R-loops (3, 8, 9), and excessive R-loop formation triggers genomic instability by stalling the progression of replication forks and by promoting DSBs (36). Therefore, we hypothesized that RNF168 may suppress excessive R-loop formation in BRCA1/2-deficient cells. To test this hypothesis, R-loop levels were assessed in MDA-MB-436 and PEO1 cells and their RNF168-depleted counterparts using single-cell microscopy coupled with immunofluorescence. RNF168 deficiency triggered significant accumulation of nuclear R-loops, as quantified using the DNA-RNA hybrid-recognizing S9.6 antibody (ref. 37 and Figure 4, A and B). Parallel to our work, a recent study has attributed DNA damage in cells lacking RNF168 and BRCA1 to a novel role of RNF168 in redundantly loading PALB2 onto damaged sites (38). We thus compared the effect of PALB2 on the levels of S9.6 in MDA-MB-436 cells. In contrast to the increased S9.6 intensity associated with RNF168 deficiency (Figure 4A), depletion of PALB2 interestingly had no significant effect on S9.6 signal when compared with shScr-transduced control cells (Supplemental Figure 7F).

To determine whether accumulation of R-loops directly accounts for genomic instability, MDA-MB-436 cells were transfected with a vector expressing RNASEH1, an enzyme that preferentially degrades RNA in DNA-RNA hybrids (3). Exogenous expression of RNASEH1 decreased the nuclear intensity of γH2AX in RNF168-deficient MDA-MB-436 cells (Figure 4C), indicative that R-loop accumulation in cells deficient for RNF168 and BRCA1 promoted their genomic instability. We then investigated whether RNF168 physically associated with R-loop–prone genomic regions. ChIP followed by quantitative PCR (ChIP-qPCR) showed enrichment of RNF168 binding at R-loop–prone *β-actin* and *ENSA* pause gene loci, as well as at rDNA loci in MDA-MB-436 cells (Supplemental Figure 8A). Importantly, knockdown of RNF168

reduced the binding signals to background levels (Figure 4D and Supplemental Figure 8B). Furthermore, RNF168 binding was also enriched at rDNA and telomeric repeats in *BRCA2*-mutant PEO1 cells (Supplemental Figure 8C). S9.6 staining of BRCA1-proficient MDA-MB-231 cells indicated that depletion of RNF168 in these cells increased their S9.6 signal intensity and elevated their DNA damage levels (Supplemental Figure 8, D and E). Notably, depletion of both RNF168 and BRCA1 in MDA-MB-231 cells led to greater DSB accumulation than observed in cells depleted of only RNF168 or BRCA1 (Supplemental Figure 5E).

Increased frequency of R-loops associated with RNF168 depletion was further corroborated in MDA-MB-436 and PEO1 cells using the DNA-RNA IP (DRIP) assay (Figure 4, E and F). The R-loop signals detected in the DRIP assays were also found to be RNASEH1 sensitive (Figure 4, E and F). In addition, ChIP-qPCR using anti-γH2AX antibody also resulted in higher enrichment of γH2AX at rDNA repeats in RNF168-depleted MDA-MB-436 cells compared with control cells, suggesting that R-loop accumulation was indeed the source of genomic instability in these cells (Supplemental Figure 8F). Most R-loops occur cotranscriptionally (3). Our analysis indicated the ability of the transcription inhibitor flavopiridol to decrease γH2AX nuclear intensity in RNF168-deficient MDA-MB-436 cells, indicating that cotranscriptional R-loops contributed to genomic instability in the absence of RNF168 and BRCA1 (Figure 4G).

BRCA1/2 maintain the stability of replication forks (39) and R-loop accumulation impairs replication fork progression (6, 7). Thus, we examined the effect of RNF168 and BRCA1 deficiency on fork progression and observed a considerably reduced fork rate in RNF168-deficient MDA-MB-436 cells (Figure 4H). Furthermore, we were able to partially, albeit nonsignificantly, rescue fork rate after RNaseH1 overexpression in RNF168-deficient MDA-MB-436 cells (Supplemental Figure 8G). Stable expression or a higher transfection efficiency rate of *RNaseH1* may have led to a statistically significant rescue of fork rate. Exposed ssDNA in R-loops can form G4 structures, DNA secondary structures that can act as barriers to fork progression and promote genomic instability (40). R-loop stability has been shown to increase when displaced ssDNA in the R-loop contains G4-DNA motifs (41). Using the QGRS Mapper G4 analysis tool (42), we examined the presence of putative quadruplex-forming G-rich sequences (QGRSs) in the displaced ssDNA. This analysis also assigns a specific G score, which is a measure of the likelihood of a QGRS forming a stable G4 structure, to the identified QGRSs (42). The analysis revealed QGRSs in the displaced ssDNA of rDNA repeats, telomeric repeats, *β-actin*, and *ENSA* pause loci (Supplemental Table 3). Interestingly, the *ENSA* pause site, which showed no significant R-loop signal in the S9.6 DRIP experiments in the absence of RNF168, also had the lowest G score. Finally, we examined the effect of RNF168 depletion on the response of MDA-MB-436 cells to pyridostatin, a G4/R-loop–stabilizing drug to which HRD cancer cells are hypersensitive (40), and found that depletion of RNF168 further sensitized *BRCA1* mutant cells to pyridostatin (Figure 4I).

Given that R-loop accumulation can lead to genomic instability through transcription-replication collisions, we examined the interaction between the transcription and replication machineries using the proximity ligation assay and antibodies against phosphorylated

serine 2 of RNA polymerase II carboxy terminal domain (CTD) and proliferating cell nuclear antigen. We found that MDA-MB-436 cells depleted of RNF168 had significantly more foci compared with control cells (Supplemental Figure 8H). Taken together, these data suggest that RNF168 suppresses R-loops and, consequently, replication stress and transcription-replication collisions associated with *BRCA1/2* mutations.

RNF168 directly ubiquitylates the helicase DHX9 to facilitate its recruitment to R-loops. To examine the mechanism underlying the role of RNF168 in *BRCA1/2*-associated cancers in greater depth, we first validated RNF168-DHX9 interactions and found that endogenous RNF168 and DHX9 coimmunoprecipitated (Figure 5A). Interaction domain-mapping assays indicated that DHX9 interacted with RNF168 through the dsRNA-binding domains (dsRBDs; Figure 5B). Although the dsRBD domains of DHX9 are not required for its unwinding function, these domains promote its binding to substrate RNA (43). Moreover, dsRBDs are thought to modulate the helicase activity of DHX9, given their role in initiating DHX9 binding to nucleic acids (44).

Concurrently, we analyzed breast cancer data from The Cancer Genome Atlas (TCGA) and observed that *RNF168* expression was positively correlated with the expression of *DHX9* (Supplemental Figure 9A). Akin to *RNF168* expression, *DHX9* was also amplified and overexpressed in the TCGA breast cancer dataset (Supplemental Figure 9A). Although DHX9 expression was not affected by RNF168 depletion (Supplemental Figure 9B), the recruitment of this helicase to R-loops at telomeric and rDNA repeats was significantly reduced in *BRCA1*-mutant MDA-MB-436 and *BRCA2*-mutant PEO1 cells (Figure 5, C and D). We next examined the effect of RNF168 depletion and overexpression on DHX9 ubiquitylation. RNF168 depletion decreased the extent of DHX9-associated Ub smears in MDA-MB-436 cells (Figure 5E), suggesting that RNF168 deficiency impaired DHX9 polyubiquitylation. Moreover, although overexpression of RNF168-WT in HEK293T cells increased DHX9 ubiquitylation, overexpression of the E3 ligase–dead RNF168-C16S mutant failed to affect ubiquitylation of DHX9 (Figure 5F).

Lysine 48 (K48) and K63-linked polyubiquitylations are major ubiquitin-associated posttranslational modifications (45). Therefore, we performed ubiquitylation assays Ub, in which all K residues except K48 or K63 were mutated to arginines. Our data indicated that RNF168 specifically promoted K63-linked polyubiquitylations of DHX9 (Figure 5G). Next, we tested whether RNF168 directly ubiquitylates DHX9 using in vitro ubiquitylation assays. Although monoubiquitylation of recombinant DHX9 was increased in the presence of recombinant RNF168, E1, E2, and Ub proteins, no smearing pattern indicative of polyubiquitylation was observed (Figure 5H). These data indicate that RNF168 directly ubiquitylates DHX9 to allow its recruitment to R-loop–enriched loci.

WT RNF168 rescues DHX9 recruitment through ubiquitylation at several lysines. To assess the functional implications of the identified DHX9-RNF168 functional relationship, RNF168-depleted MDA-MB-436 cells and their counterparts reconstituted with RNF168-WT or RNF168-C16S were examined for DHX9 recruitment to R-loop–prone loci. RNF168-WT, but not RNF168-C16S, restored DHX9 recruitment to these loci in RNF168-depleted cells (Figure 6A). Consistently, depletion of DHX9 in MDA-MB-436 cells increased S9.6

signal intensity and DSB levels and resulted in cellular phenotypes similar to RNF168-knockdown cells (Figure 6B and Supplemental Figure 9, C and D). In turn, knockdown of both RNF168 and DHX9 in these cells did not significantly increase DSB levels (Figure 6B). Taken together, these data suggest that RNF168-dependent ubiquitylation of DHX9 promotes the recruitment of this helicase to R-loop–prone loci, thereby promoting the resolution of DNA-RNA hybrid structures and suppressing genomic instability.

To identify sites of DHX9 ubiquitylation by RNF168, in vitro ubiquitylation assays combined with mass-spectrometry analyses were used. RNF168 was found to directly ubiquitylate DHX9 at 12 distinct lysines (Supplemental Table 4). Given the role of the helicase domain of DHX9 in R-loop resolution, we mutated 2 lysines (K) found to be ubiquitylated by RNF168 within the helicase domain, K697 and K708, to arginines (KXR) and evaluated their impact on DHX9 stability, recruitment to R-loop–prone genomic loci, and activity at these loci. ChIP-qPCR results indicated that both DHX9 mutants displayed decreased recruitment to all examined R-loop–prone loci compared with DHX9-WT (Figure 6C). DRIP-qPCR in HEK293T cells overexpressing K697R and K708R DHX9 mutants showed a moderate S9.6 enrichment to R-loop–prone genomic loci when compared with cells overexpressing DHX9-WT, with significant enrichment at rDNA repeats in cells overexpressing K708R (Figure 6D). Finally, MDA-MB-436 cells expressing DHX9 mutants DHX9-K697R and -K708R displayed an increase in S9.6 intensity when compared with DHX9-WT–expressing cells indicative of greater R-loop formation (Figure 6E). These data suggest that loss of RNF168 ubiquitylation of DHX9 at its helicase domain (K697 and K708) impairs both DHX9 recruitment to R-loops and its ability to resolve these structures.

Discussion

Targeting DNA repair deficiency for cancer therapy has led to the identification and approval of PARPi for the treatment of locally advanced or metastatic breast cancer with germline *BRCA1/2* mutations, as well as chemoresistant and recurrent *BRCA1/2*-mutant ovarian cancer. Unfortunately, intrinsic or acquired resistance to PARPi is common (1). Our study identified a dependence on the survival of *BRCA1/2*-deficient tumors on mechanisms that suppress genomic instability through R-loop resolution. We describe a fundamental role for RNF168 in the regulation of genomic instability caused by R-loops in cells deficient in BRCA1 or BRCA2. The molecular mechanism underlying this function is based on increased R-loop accumulation due to defective ubiquitylation of the helicase DHX9 in the absence of RNF168. Consequently, loss of RNF168 severely reduces proliferation of cells that exhibit loss of function of BRCA1/2 and protects against tumorigenesis associated with *BRCA1/2* mutations (Figure 7). This mechanism is corroborated by the loss of viability observed in *BRCA1*-deficient cells lacking DHX9. Further, our mouse models demonstrated that Rnf168 depletion protected against *Brca1*-mutated mammary tumorigenesis, and we have identified a human genetic variant that may reduce breast cancer risk in *BRCA1* mutation carriers and is associated with reduced *RNF168* expression. This may potentially play a role in driving decisions regarding recommendations for prophylactic mastectomy and/or oophorectomy in *BRCA1* mutation carriers; however, further examination is warranted.

Here, we demonstrated defective homologous recombination repair in cells deficient for RNF168 and BRCA1. This is consistent with a recent report in which depletion of RNF168 in BRCA1-deficient cells caused loss of residual loading of the homologous recombination factor RAD51 (38). Although this study has shown a role for RNF168 in redundantly loading the homologous recombination factor PALB2 onto DNA break sites, the potentially novel RNF168 function in R-loop resolution identified here appears to be independent of PALB2. In our model system, we observed that in contrast to RNF168, depletion of PALB2 did not promote accumulation of R-loops in *BRCA1* mutant cells. It has also previously been shown that RAD51 depletion does not result in accumulation of R-loops as detected by DRIP (9), suggesting that RNF168 prevents R-loop accumulation independently of its role in PALB2-BRCA2-RAD51 loading in a BRCA1-deficient setting.

Zong et al. also reported that loss of RNF168 led to homologous recombination restoration in *Brca1*$^{A2/A2}$ mice that express a RING-less BRCA1; however, homologous recombination and viability were further reduced in *Rnf168*$^{-/-}$ *Brca1*$^{A11/A11}$ cells (38). *Brca1*$^{fl/fl}$ mice used in our study had *loxP* sites flanking exons 5 and 6. After Cre expression, exon 5 and 6 deletion resulted in cells that were null for the Brca1 gene and that showed elevated levels of γH2AX, suggesting that the observed protection against mammary tumorigenesis in our DKO mice was unlikely due to restoration of homologous recombination. Our results are consistent with another recent study, which showed that although complete loss of RNF168 and BRCA1 resulted in efficient DNA end resection, loss of PALB2-BRCA2-RAD51 loading diminished residual homologous recombination, consequently leading to cell unviability (46). Overexpression of RNF168 in a BRCA1-deficient setting has been shown to abolish end resection through robust 53BP1 recruitment and inhibition of end resection (46), suggesting that a balance of RNF168 expression is essential for the viability of BRCA1-deficient tumors. It is likely that DNA damage caused by R-loop accumulation in the absence of RNF168 and BRCA1 is not repaired due to the loss of PALB2-BRCA2-RAD51 loading, highlighting multiple functions of RNF168 in maintaining genomic stability in BRCA1-deficient tumor cells.

We have also identified a mechanism by which RNF168 ubiquitylates DHX9 and have identified that RNF168 directly ubiquitylated DHX9 at K697 and K708. In BRCA1/2-deficient cells, RNF168 ubiquitylated these sites to facilitate the recruitment of DHX9 to R-loops. This mechanism restrained excessive accumulation of R-loops, which can compromise genomic integrity and replication fork stability. Interestingly, both K697 and K708 are located within the DHX9 core helicase domains. Although mutation of these lysines to arginine minimally affected DHX9 stability, our results indicated that it hampered DHX9 recruitment to R-loop–prone genomic loci and globally elevated S9.6 intensity and DRIP enrichment at aforementioned loci. Consequently, loss of RNF168 in BRCA1/2-deficient cells led to R-loop accumulation and cell death. Although it is plausible that impaired R-loop resolution associated with DHX9 substitutions K697R and K708R may not only be due to the loss of DHX9 ubiquitylation, specifically at these sites, the role of RNF168 in ubiquitylating DHX9 and recruiting it to R-loops is evident based on our data.

R-loops can be stabilized if the displaced ssDNA is prone to forming G4 structures (47, 48). The displaced ssDNA at the genomic loci examined in this study was indeed prone to forming G4 structures, explaining the increased sensitivity of RNF168-deficient MDA-MB-436 cells to the G4-stabilizing drug pyridostatin. Our results highlighting R-loop exacerbation as a mechanism restraining growth of BRCA1/2-deficient tumors are consistent with the recent data showing that increased DNA damage and genomic instability in cells treated with G4 ligands (e.g., pyridostatin) are mediated through R-loops (49). In addition to DHX9 ubiquitylation shown here, RNF168 was found to ubiquitylate the G4-resolving helicase BLM to trigger its recruitment to stalled replication forks (50). Furthermore, both DHX9 and BLM have been individually implicated in regulating R-loop-associated DNA damage (51, 52). Thus, although our data strongly support a major role for RNF168 in DHX9-mediated R-loop resolution in BRCA1/2-deficient cells, RNF168-mediated BLM regulation may also contribute to R-loop resolution in BRCA1/2-deficient cells. It is also plausible that other R-loop factors and putative RNF168 interactors, such as DDX21, may be deregulated in the absence of RNF168, thus also contributing to R-loop accumulation.

In this study, we observed association of the SNP rs192573104 with reduced levels of *RNF168* expression and decreased breast cancer penetrance in *BRCA1* mutation carriers. This is consistent with our finding in mouse models that RNF168 loss markedly suppressed mammary tumorigenesis associated with *Brca1* mutations, implicating RNF168 as a potential target for reducing cancer risk in *BRCA1* mutation carriers. In the absence of drugs or compounds targeting RNF168, exacerbation of R-loop accumulation by other means should be addressed relative to the toxicity and efficacy in preclinical preventive settings. At the somatic level, impaired growth of *BRCA1/2*-mutant breast and ovarian cancer cells in vitro and in vivo, and their increased sensitivity to PARPi after depletion of RNF168, suggest that RNF168 is a promising therapeutic target for these cancers.

Collectively, our data reveal RNF168 as a major player in suppressing *BRCA1/2*-mutant cancers by facilitating R-loop resolution through the recruitment of DHX9 to these structures. Potential RNF168 targeting may expose further vulnerability of *BRCA1/2* cancers and other HRD cancers toward the development of therapeutic strategies complementing current chemotherapy and PARP-targeting approaches.

Methods

Further information can be found in the Supplemental Methods.

Bioinformatic analysis. Preprocessed and normalized gene expression (RNA-Seq) and copy number data in normal tissue and cancer samples and corresponding clinical and pathological information were taken from The Cancer Genome Atlas (TCGA) repository (GDC Data Portal) and relevant publications (53, 54). Individual-level data, including those relating to somatic mutations and germline genetic variation, were obtained with approval from the Data Access Committee (project 11689). Cox regression survival analyses were performed using the R survival package, and multivariate analyses included age at diagnosis and tumor stage. Pearson correlation coefficients and their corresponding *P* values and scatter plots were obtained using R functions. The canonical PAM50 signature was used to identify

breast cancer subtypes in unsupervised hierarchical clustering, and the results were compared with those from tumors classified according to their expression of *ESR1*, *ERBB2*, and *PR* categorized into tertiles. Hierarchical clustering trees were obtained by Ward's method and from Euclidean distances, using standardized values and the heatmap.3 package. Mutational signatures were defined using the deconstructSigs (55) package and MuTect somatic mutations in GDC (September 13, 2017). Oncoprints corresponding to mRNA expression *z* scores and genetic alteration data for TCGA Breast Cancer Provisional and Ovarian Serous Cystadenocarcinoma Provisional datasets were downloaded from cBioPortal for Cancer Genomics.

Modification of cancer risk. This analysis was performed using data from the OncoArray and iCOGS consortia with the participation of CIMBA. The OncoArray and iCOGS designs, quality controls, and statistical analyses have been described elsewhere (24–26). The associations were assessed using the 1 degree of freedom score test statistic based on a retrospective likelihood method that adjusts for the nonrandom sampling of mutation carriers with respect to their disease status. To allow for nonindependence among related individuals, the correlation between the genotypes was taken into account using a kinship-adjusted version of the test score statistic. The *P* values presented were based on the adjusted test score. To estimate HRs, the effect of each SNP was modeled per allele or per genotype on the log scale by maximizing the retrospective likelihood.

Mice. $Brca1^{fl/fl}$ (*loxP* sites flanking exons 5 and 6) conditional mutant mice (18) were crossed with transgenic *Wap-Cre* mice (The Jackson Laboratory) to obtain *Wap-Cre* $Brca1^{fl/fl}$ mice. $Rnf168^{-/-}$ mice (19) were crossed with *Wap-Cre* $Brca1^{fl/fl}$ mice to generate $Rnf168^{-/-}$ *Wap-Cre* $Brca1^{fl/fl}$ females. A power analysis was performed to estimate the minimum number of female mice needed to ensure 80% statistical power for comparing $Rnf168^{-/-}$ *Wap-Cre* $Brca1^{fl/fl}$ and *Wap-Cre* $Brca1^{fl/fl}$ in a survival analysis. WT and $Brca1^{fl/fl}$ females were used as experimental controls. Mice in this study had a mixed 129/J–C57BL/6 genetic background and were genotyped by PCR. Mice were housed in a pathogen-free mouse facility at the Princess Margaret Cancer Centre (PMCC), and all procedures were performed in compliance with the PMCC Animal Care Committee guidelines. Investigators were not blinded to the genotypes of mice. Survival cohorts of female mice were monitored for mammary tumor onset by palpation as well as for signs of other tumors once a week for more than 600 days. The log-rank test, performed using GraphPad Prism 7 (GraphPad Software), was used to determine statistically significant differences between survival curves.

Cell lines and cell culture. 3T3-immortalized MEFs were generated following standard protocols. Primary mouse MECs were prepared as previously described (56) and immortalized using pBabe-zeo large TcDNA (Addgene plasmid 1779). These cells, as well as MDA-MB-436 cells and HEK293T cells (ATCC), were cultured in DMEM (GIBCO) supplemented with 10% FBS, 5×10^{-5} M 2-ME, 100 U/mL penicillin, and 100 μg/mL streptomycin (complete DMEM). PEO1 cells, obtained from R. Rottapel (Princess Margaret Cancer Centre, University Health Network, Toronto, Ontario, Canada), and HCC1937 (ATCC) cells were cultured in RPMI (GIBCO) supplemented with 10% FBS, 5×10^{-5} M 2-ME, 100 μ/mL penicillin, and 100 μg/mL streptomycin (complete RPMI). All cell lines were tested to be mycoplasma-free. All cells were maintained in a humidified atmosphere at 37°C and 5% CO_2. MDA-MB-436 and PEO1 cells were authenticated by short tandem repeat (STR) profiling. For lentiviral preparation, HEK293T cells were cotransfected by calcium phosphate

precipitation with shRNA containing lentivirus constructs or pLenti-CMV-LUC (Addgene plasmid 17477) together with psPAX-2 (Addgene plasmid 12260) and pMD2.G (Addgene plasmid 12259). Human breast cancer cell lines MDA-MB-436, HCC1937, and PEO1 cells were transduced with pLKO.1-Puro (Addgene plasmid 8453), pLKO.1-blast (Addgene plasmid 26655), or Tet-pLKO-Puro (Addgene plasmid 21915) lentiviruses encoding shRNAs targeting human *RNF168* (shRNA 1; 5′-GAAGAGTCGTGCCTACTGATT-3′; shRNA 2; TRCN0000034137: 5′-GCAGTCAGTTAATAGAAGAAA-3′), or mouse *Rnf168* (shRNA 1; TCRN00000040876: 5′-CCTTGGCTTCTCCTTTGAGTT-3′; shRNA 2; TCRN00000040877: 5′-CTGGACAAGAATCAAAGGAAA-3′), shBRCA1: 5′- GAGTATGCAAACAGCTATAAT-3′), and shPALB2: 5′-GGCCTTTCTTCATCCATATTA-3′. Glycerol stocks of the shDHX9 construct were ordered from Sigma-Aldrich (TRCN0000350304). As a control, cells were transduced with lentiviral particles carrying the corresponding scramble shRNA. The expression of RNF168 was examined by Western blotting using anti-RNF168 antibody (R&D Systems, AF7217). The expression of BRCA1 was examined by Western blotting using anti-BRCA1 antibody (Abcam, 16780). The expression of DHX9 and PALB2 was examined by Western blotting using anti-DHX9 antibody (Bethyl, A300-855A) and anti-PALB2 antibody (Bethyl, A301-246A), respectively. Mouse BRCA1 was detected using a homemade rabbit polyclonal antibody that we generated against mouse BRCA1 peptide 1071-1081. β-actin was used as a loading control for Western blots and detected using anti–β-actin antibody (Santa Cruz Biotechnology, SC-47778).

DSB repair assays. To determine homologous recombination, NHEJ, and a-EJ efficiency, constructs containing homologous recombination or NHEJ (28) or a-EJ (29) reporter cassettes were linearized with the I-SceI restriction enzyme (NEB) and transfected into human breast cancer cell lines using a GenJet in vitro DNA transfection kit (SignaGen Laboratories). The red fluorescent protein (RFP) construct was cotransfected as an internal control. Transfected cells were examined 48 hours later by flow cytometry (BD Biosciences FACSCanto) to determine their levels of EGFP and RFP expression. Analyses were performed using FlowJo 10. Repair efficiencies of experimental samples were normalized relative to the control.

Immunofluorescence. Immunofluorescence staining for subnuclear foci formation was performed in MEFs and human cell lines as previously described (16). Primary antibodies used for immunofluorescence staining were 1:600 for anti-γH2AX (MilliporeSigma, 05-636 JBW301), 1:1000 anti-TP53BP1 (Bethyl, A300-272), and 7.5 μg in 1000 anti-Flag (MilliporeSigma, F7425). Anti-rabbit or anti-mouse IgG conjugated with Alexa Fluor 488 or 594 (Invitrogen) was used for secondary staining. Subsequently, slides were counterstained with DAPI (Invitrogen) and mounted using Mowiol (Sigma-Aldrich). Images were taken using a Leica (DM4000B) fluorescence microscope under 63× or 100× magnification. For R-loop microscopy analysis, 40,000 MDA-MB-436 cells transduced with shScr or sh*RNF168* were seeded onto coverslips coated with poly-L-lysine (PLL). For RNASEH1 overexpression analysis, cells were first seeded in 6-well plates and transfected 24 hours later with 2 μg pcDNA3-Empty or pcDNA3-*RNASEH1*. Next, 48 hours after transfection, cells were harvested and reseeded onto PLL-coated coverslips, which were processed after a further 24 hours using anti-γH2AX and anti-RNASEH1 antibodies to assess DSBs and confirm successful RNASEH1 overexpression, respectively. For experiments assessing the impact of transcriptional inhibition, cells transduced with sh*RNF168* were seeded onto coverslips, treated for 2

hours with vehicle control or flavopiridol (2 μM; Santa Cruz Biotechnology), and then processed for γH2AX immunofluorescence, which was carried out on cells grown on coverslips in 24-well plates. Cells were fixed with 1% formaldehyde (15 minutes), washed 3 times with 1× PBS, permeabilized with 0.3% Triton X-100, and washed 3 additional times. Coverslips were blocked using 5% BSA and transferred to humidified chambers. Coverslips were incubated with 60 μL of primary antibody for 1 hour at the following concentrations: 1:250 anti-RNASEH1 (Proteintech, 15606-1-AP) or 1:500 anti–DNA-RNA hybrid S9.6 (Kerafast, ENH001). Coverslips were washed 3 times with 1× PBS and incubated with fluorophore-conjugated secondary antibodies. Subsequently, coverslips were washed 4 times with 1× PBS and subjected to nuclear staining using DAPI, mounted in DAKO fluorescent mounting medium on microscope slides, and sealed with nail polish. For RNA-DNA-hybrid or γH2AX/RNASEH1 microscopy (following RNASEH1 overexpression), we employed a Nikon C2+ confocal microscope coupled to NIS-Elements AR software (Nikon). Random fields at 100× magnification were identified by DAPI staining. For each image, 5–7 2D imaging planes were acquired along the z axis. To assess the nuclear signal for R-loops, γH2AX, or RNASEH1, the DAPI signal was first used to create masks of nuclei, and MFI values for cells were obtained by scrolling through 2D planes. For RNA-DNA-hybrid/Flag and γH2AX microscopy, images were acquired at 100× magnification on a Leica DM4000B fluorescence microscope and quantified using ImageJ (NIH).

Intracellular ubiquitylation assay. HEK293T cells were transfected with *Rnf168-Flag* or *Rnf168^{C16S}-Flag* and WT or mutated Ub-HA (Addgene plasmids pRK5-HA-Ub-WT [ID 17608], pRK5-HA-Ub-K48 [ID 17605], pRK5-HA-Ub-K63 [ID 17606]) as indicated. Then, 48 hours later, cell lysates were prepared, precleared with protein A Sepharose beads (Life Technologies, Thermo Fisher Scientific), and subjected to IP using anti–DHX-9 (Bethyl, A300-855A). Subsequently, the beads were washed, and proteins were released from them by boiling in 2× SDS-PAGE sample buffer. Immunoblot analysis was performed using the indicated antibodies.

In vivo ubiquitylation assay. MDA-MB-436 cancer cells with RNF168-KD and control cell ubiquitylation levels of DHX9 were examined using the in vivo ubiquitylation assay, as previously described (21).

In vitro ubiquitination assay. Recombinant RNF168 (1.5 μg), recombinant DHX9 (5 μg), UBE1 (0.1 μg; E1), UBE2E2 (0.2 μg; E2), HA-Ub (5 μg), and ATP (2.5 mM) were mixed and the reactions were incubated at 30 °C for 90 minutes in buffer containing 50 mM Tris/HCl (pH 7.5), 5 mM MgCl$_2$, and 2mM DTT and examined though Western blotting using anti-ubiquitin antibody (Sigma-Aldrich, clone 6C1- U0508) or run on an SDS-PAGE gel for mass spectrometry.

Statistics. The 2-tailed, unpaired samples Student's t test was performed to compare pairs of group means. The researchers were blinded to the identity of the specific sample during the experiment and when assessing the outcome whenever the nature of the experiments permitted it. The log-rank test was used to compare survival curves from mouse models and patients with breast cancer. Statistical analyses were carried out with GraphPad Prism 7. A P value less than 0.05 was considered statistically significant.

Study approval. All experimental procedures using mice were reviewed and approved by the PMCC Animal Care Committee. All experiments involving viruses were approved by the University Health Network Biosafety Committee (University of Toronto, Toronto, Ontario, Canada).

Author contributions

PSP and RH designed the study. PSP, KJA, KKNG, MJH, ZK, BH, SD, JSG, AA, FM, SEG, HB, and AH performed experiments. LP and MAP performed bioinformatic analyses. DRB, JB, GCT, ACA, and MAP identified rs192573104. OS examined tumors and biopsies. HKB shared reagents and reviewed the manuscript. GWB supervised BH, MAP supervised LP and FM, EBA supervised HB, CHA supervised SD, KM supervised KJA, BR supervised JSG, and RH supervised PSP, KKNG, ZK, AA, and AH. The manuscript was written by PSP, KJA, MAP, KM, AH, and RH.

1. Ashworth A, Lord CJ. Synthetic lethal therapies for cancer: what's next after PARP inhibitors? *Nat Rev Clin Oncol*. 2018;15(9):564–576.

2. Prakash R, et al. Homologous recombination and human health: the roles of BRCA1, BRCA2, and associated proteins. *Cold Spring Harb Perspect Biol*. 2015;7(4):a016600.

3. Garcia-Muse T, Aguilera A. R loops: from physiological to pathological roles. *Cell*. 2019;179(3):604–618.

4. Balk B, et al. Telomeric RNA-DNA hybrids affect telomere-length dynamics and senescence. *Nat Struct Mol Biol*. 2013;20(10):1199–1205.

5. Skourti-Stathaki K, Proudfoot NJ. A double-edged sword: R loops as threats to genome integrity and powerful regulators of gene expression. *Genes Dev*. 2014;28(13):1384–1396.

6. Chan YA, et al. Mechanisms of genome instability induced by RNA-processing defects. *Trends Genet*. 2014;30(6):245–253.

7. Madireddy A, et al. FANCD2 facilitates replication through common fragile sites. *Mol Cell*. 2016;64(2):388–404.

8. Hatchi E, et al. BRCA1 recruitment to transcriptional pause sites is required for R-loop-driven DNA damage repair. *Mol Cell*. 2015;57(4):636–647.

9. Bhatia V, et al. BRCA2 prevents R-loop accumulation and associates with TREX-2 mRNA export factor PCID2. *Nature*. 2014;511(7509):362–365.

10. Shivji MKK, et al. BRCA2 regulates transcription elongation by RNA polymerase II to prevent R-loop accumulation. *Cell Rep*. 2018;22(4):1031–1039.

11. Zhang X, et al. Attenuation of RNA polymerase II pausing mitigates BRCA1-associated R-loop accumulation and tumorigenesis. *Nat Commun*. 2017;8:15908.

12. Molyneux G, et al. BRCA1 basal-like breast cancers originate from luminal epithelial progenitors and not from basal stem cells. *Cell Stem Cell*. 2010;7(3):403–417.

13. Brown JS, et al. Targeting DNA repair in cancer: beyond PARP inhibitors. *Cancer Discov*. 2017;7(1):20–37.

14. Bouwman P, et al. 53BP1 loss rescues BRCA1 deficiency and is associated with triple-negative and BRCA-mutated breast cancers. *Nat Struct Mol Biol*. 2010;17(6):688–695.

15. Bunting SF, et al. 53BP1 inhibits homologous recombination in Brca1-deficient cells by blocking resection of DNA breaks. *Cell*. 2010;141(2):243–254.

16. Bohgaki M, et al. RNF168 ubiquitylates 53BP1 and controls its response to DNA double-strand breaks. *Proc Natl Acad Sci U S A*. 2013;110(52):20982–20987.

17. Schwertman P, et al. Regulation of DNA double-strand break repair by ubiquitin and ubiquitin-like modifiers. *Nat Rev Mol Cell Biol*. 2016;17(6):379–394.

18. McPherson JP, et al. Collaboration of Brca1 and Chk2 in tumorigenesis. *Genes Dev*. 2004;18(10):1144–1153.

19. Bohgaki T, et al. Genomic instability, defective spermatogenesis, immunodeficiency, and cancer in a mouse model of the RIDDLE syndrome. *PLoS Genet*. 2011;7(4):e1001381.

20. Mak TW, et al. Brca1 required for T cell lineage development but not TCR loci rearrangement. *Nat Immunol*. 2000;1(1):77–82.

21. Guturi KK, et al. RNF168 and USP10 regulate topoisomerase IIα function via opposing effects on its ubiquitylation. *Nat Commun*. 2016;7:12638.

22. Cerami E, et al. The cBio cancer genomics portal: an open platform for exploring multidimensional cancer genomics data. *Cancer Discov*. 2012;2(5):401–404.

23. Alexandrov LB, et al. Signatures of mutational processes in human cancer. *Nature*. 2013;500(7463):415–421.

24. Couch FJ, et al. Genome-wide association study in BRCA1 mutation carriers identifies novel loci associated with breast and ovarian cancer risk. *PLoS Genet*. 2013;9(3):e1003212.

25. Gaudet MM, et al. Identification of a BRCA2-specific modifier locus at 6p24 related to breast cancer risk. *PLoS Genet*. 2013;9(3):e1003173.

26. Milne RL, et al. Identification of ten variants associated with risk of estrogen-receptor-negative breast cancer. *Nat Genet*. 2017;49(12):1767–1778.

27. GTEx Consortium, et al. Genetic effects on gene expression across human tissues. *Nature*. 2017;550(7675):204–213.

28. Mao Z, et al. DNA repair by homologous recombination, but not by nonhomologous end joining, is elevated in breast cancer cells. *Neoplasia*. 2009;11(7):683–691.

29. Bennardo N, et al. Alternative-NHEJ is a mechanistically distinct pathway of mammalian chromosome break repair. *PLoS Genet*. 2008;4(6):e1000110.

30. Kuilman T, et al. The essence of senescence. *Genes Dev*. 2010;24(22):2463–2479.

31. Sharpless NE, Sherr CJ. Forging a signature of in vivo senescence. *Nat Rev Cancer*. 2015;15(7):397–408.

32. Kass EM, et al. When genome maintenance goes badly awry. *Mol Cell*. 2016;62(5):777–787.

33. Roy R, et al. BRCA1 and BRCA2: different roles in a common pathway of genome protection. *Nat Rev Cancer*. 2011;12(1):68–78.

34. Jain A, et al. DHX9 helicase is involved in preventing genomic instability induced by alternatively structured DNA in human cells. *Nucleic Acids Res*. 2013;41(22):10345–10357.

35. Chakraborty P, Grosse F. Human DHX9 helicase preferentially unwinds RNA-containing displacement loops (R-loops) and G-quadruplexes. *DNA Repair (Amst)*. 2011;10(6):654–665.

36. Gan W, et al. R-loop-mediated genomic instability is caused by impairment of replication fork progression. *Genes Dev*. 2011;25(19):2041–2056.

37. Atchley DP, et al. Clinical and pathologic characteristics of patients with BRCA-positive and BRCA-negative breast cancer. *J Clin Oncol*. 2008;26(26):4282–4288.

38. Zong D, et al. BRCA1 haploinsufficiency is masked by RNF168-mediated chromatin ubiquitylation. *Mol Cell*. 2019;73(6):1267–1281.e7.

39. Berti M, Vindigni A. Replication stress: getting back on track. *Nat Struct Mol Biol*. 2016;23(2):103–109.

40. Zimmer J, et al. Targeting BRCA1 and BRCA2 deficiencies with G-quadruplex-interacting compounds. *Mol Cell*. 2016;61(3):449–460.

41. Salvi JS, et al. Roles for Pbp1 and caloric restriction in genome and lifespan maintenance via suppression of RNA-DNA hybrids. *Dev Cell*. 2014;30(2):177–191.

42. Kikin O, et al. QGRS Mapper: a web-based server for predicting G-quadruplexes in nucleotide sequences. *Nucleic Acids Res*. 2006;34(Web Server issue):W676–W682.

43. Xing L, et al. Helicase associated 2 domain is essential for helicase activity of RNA helicase A. *Biochim Biophys Acta*. 2014;1844(10):1757–1764.

44. Zhang S, Grosse F. Domain structure of human nuclear DNA helicase II (RNA helicase A). *J Biol Chem*. 1997;272(17):11487–11494.

45. Akutsu M, et al. Ubiquitin chain diversity at a glance. *J Cell Sci*. 2016;129(5):875–880.

46. Krais JJ, et al. RNF168-mediated ubiquitin signaling inhibits the viability of *BRCA1*-null cancers. *Cancer Res*. 2020;80(13):2848–2860.

47. Duquette ML, et al. Intracellular transcription of G-rich DNAs induces formation of G-loops, novel structures containing G4 DNA. *Genes Dev*. 2004;18(13):1618–1629.

48. Salvi JS, Mekhail K. R-loops highlight the nucleus in ALS. *Nucleus*. 2015;6(1):23–29.

49. De Magis A, et al. DNA damage and genome instability by G-quadruplex ligands are mediated by R loops in human cancer cells. *Proc Natl Acad Sci U S A*. 2019;116(3):816–825.

50. Tikoo S, et al. Ubiquitin-dependent recruitment of the Bloom syndrome helicase upon replication stress is required to suppress homologous recombination. *EMBO J*. 2013;32(12):1778–1792.

51. Chang EY, et al. RECQ-like helicases Sgs1 and BLM regulate R-loop-associated genome instability. *J Cell Biol*. 2017;216(12):3991–4005.

52. Cristini A, et al. RNA/DNA hybrid interactome identifies DXH9 as a molecular player in transcriptional termination and R-loop-associated DNA damage. *Cell Rep*. 2018;23(6):1891–1905.

53. Cancer Genome Atlas N. Comprehensive molecular portraits of human breast tumours. *Nature*. 2012;490(7418):61–70.

54. Ciriello G, et al. Comprehensive molecular portraits of invasive lobular breast cancer. *Cell*. 2015;163(2):506–519.

55. Rosenthal R, et al. DeconstructSigs: delineating mutational processes in single tumors distinguishes DNA repair deficiencies and patterns of carcinoma evolution. *Genome Biol*. 2016;17:31.

56. Li L, et al. Ubiquitin ligase RNF8 suppresses Notch signaling to regulate mammary development and tumorigenesis. *J Clin Invest*. 2018;128(10):4525–4542.